ACS APPLIED MATERIALS & INTERFACES

Research Article

www.acsami.org

Enhanced Photoresponse in Monolayer Hydrogenated Graphene Photodetector

Prarthana Gowda,[†] Dipti R. Mohapatra,[‡] and Abha Misra*[,†]

[†]Department of Instrumentation and Applied Physics, [‡]Department of Physics, Indian Institute of Science, Bangalore, India 560012

ABSTRACT: We report the photoresponse of a hydrogenated graphene (H-graphene)-based infrared (IR) photodetector that is 4 times higher than that of pristine graphene. An enhanced photoresponse in H-graphene is attributed to the longer photoinduced carrier lifetime and hence a higher internal quantum efficiency of the device. Moreover, a variation in the angle of incidence of IR radiation demonstrated a nonlinear photoresponse of the detector, which can be attributed to the photon drag effect. However, a linear dependence of the photoresponse is revealed with different incident powers for a given angle of IR incidence. This study presents H-graphene as a tunable photodetector for advanced photoelectronic devices with higher responsivity. In addition, in situ tunability of the graphene bandgap enables achieving a cost-effective technique for developing photodetectors without involving any external treatments.

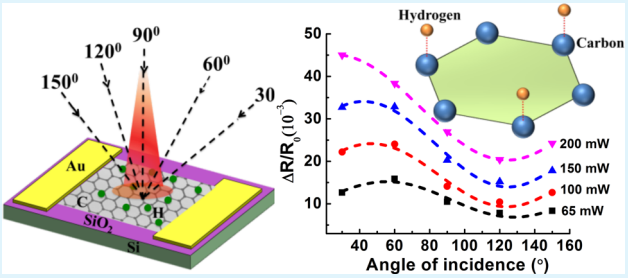

KEYWORDS: *H-graphene, infrared, photodetectors, angle of incidence, hydrogenation*

1. INTRODUCTION

Graphene has demonstrated a great promise for ultrabroadband (~500 GHz) photodetection with a fast response time of ~1.5 ps due to its gapless band structure.[1−4] However, a very short lifetime of photogenerated carriers limits its quantum efficiency to below 30% and responsivity to 0.1A/W.[5] Therefore, in order to efficiently generate the photocurrent, it is essential to separate the generated electrons and holes on a subpicosecond time scale.[6] The sensing scheme offered in most of the reported graphene photodetectors exploit either hybrid structures,[7] graphene-metal junctions,[8,9] or graphene p−n junctions[10,11] for enhancement in the photocurrent, which experiences a smaller effective junction area for overall lower optical absorption and hence still faces a limited responsivity as compared to the other materials like InAs−InGaAs quantum dot.[12] Moreover, all of these studies were based on field effect transistors containing exfoliated graphene that are not suitable for large-area applications.[13] Therefore, band structure engineering of large-area graphene has recently been attempted to enhance photoresponsivity.[14,15] Subsequently, chemical functionalization[16,17] and doping[18,19] of graphene have presented promising methods for tuning the band gap in graphene. In particular, chemical binding of hydrogen to the graphene lattice transforms the sp^2 hybridization to sp^3, which in turn opens the band gap by removing the conducting π-bond.[20] The band gap can be further tuned by controlling the amount of hydrogen bonding to the surface of graphene.[21] In addition, hydrogenated graphene (H-graphene) shows reversible characteristics of the metallic state after hydrogen is removed from the lattice, as was described by Elias et al.[22] Thus, H-graphene could present the requisite photocarrier lifetime, similar to that of conventional semiconductors, while achieving better photoresponse. There is no report to date on the H-graphene photodetector, which is the motivation of present study. In this report, we present H-graphene as a novel photodetector material for infrared (IR) sensing. This study reveals a strong optical angle dependence, which greatly impacts the photoresponse of the H-graphene and presents its tunable characteristics by injecting a variable optical power.

Graphene was synthesized on a copper foil by chemical vapor deposition (CVD). Exposing graphene to the hydrogen plasma for 2s enabled hydrogen functionalization of graphene. A detailed growth procedure is described in the Experimental Methods.

Figure 1a,b shows the Raman spectra of both pristine and H-graphene samples. In Figure 1a, the pristine graphene shows a 2D band at 2678 cm^{-1} and a G band at 1583 cm^{-1}. The G band corresponds to the in-plane vibration of optical E_{2g} phonons at the Brillion zone center, whereas the 2D band is a two-phonon intervalley double resonance scattering of a transverse optic (TO) phonon. The intensity ratio of 2D to G bands (I_{2D}/I_G) is ~2.4, which indicates single-layer graphene. The peak at 1342 cm^{-1} is a defect mediated D band induced by the double resonance of the TO phonon and a defect at the K-point of the Brillion zone center. The relatively weak intensity of the D band (I_D/I_G ~ 0.18) illustrates a high quality of the graphene. Figure 1b depicts the Raman spectra of the hydrogen plasma treated graphene; a substantial increase in the intensity of the D band is demonstrated, while the 2D band almost disappeared, which signifies the attachment of hydrogen to the graphene

Received: June 18, 2014
Accepted: September 11, 2014
Published: September 11, 2014

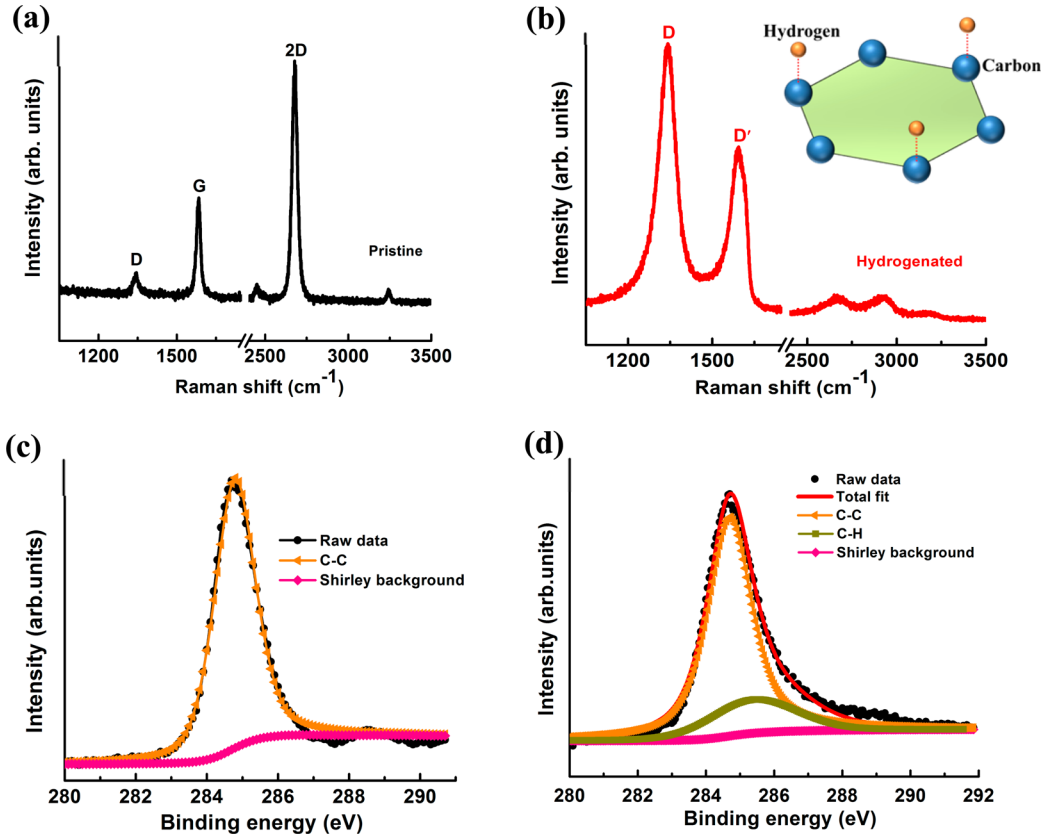

Figure 1. Raman spectra of single-layer graphene (a) before hydrogenation and (b) after hydrogenation; (b, inset) schematic of the hydrogen-incorporated graphene lattice. C1s core-level XPS spectra of single-layer graphene (c) before hydrogenation and (d) after hydrogenation.

lattice. Moreover, two new modes appear; one is at 1615 cm^{-1}, known as D′ band, due to the intervalley double resonance process in the presence of defects, the second new mode is at 2930 cm^{-1} that is a combination of both D and G modes, known as D + G mode. Therefore, an increase in D band intensity and the emergence of new disorder-induced peaks activated by hydrogenation of graphene indicated the presence of point defects mostly related to C−H sp^3 bonding, which breaks the translation invariance in the pristine graphene.[22] From the intensity ratio of D to G bands of H-graphene, I_D/I_G ~1.6, the average distance between the defects, L_D, is estimated to be ~1.7 nm, using an empirical relationship[23−25] that corresponds to the size of the defect free area or sp^2 hybridized island.

H-graphene was further characterized by X-ray photoemission spectroscopy (XPS). Figure 1c,d illustrates the C1s core level spectra of pristine (without hydrogen treatment) and hydrogen plasma treated graphene, respectively. The XPS spectra of the pristine graphene can only be fitted with a single peak at binding energy (BE) of 284.7 eV corresponding to sp^2 hybridized carbon atom (C−C bond) in the graphene. In contrast, the C1s spectrum of H-graphene is fitted with two peaks−a higher intensity peak at 284.7 eV, which is similar to that of the pristine graphene and the second peak is at higher BE of 285.2 eV that is assigned to the sp^3 hybridized C-atoms due to the formation of C−H bond after hydrogen plasma treatment. Hence, it is clear that H-graphene contains both the sp^2 and sp^3 phases due to nonuniform attachment of hydrogen in the carbon lattice. The hydrogen coverage in H-graphene was calculated to be 33% from the intensity ratio of sp^3 and sp^2-hybridized C-components of the C1s spectra. Moreover, a lattice mismatch between copper substrate and graphene causes a shift in both the peaks by 0.2 eV as compared to the reported values.[26]

Photoresponse of the H-graphene device was measured in two different experiments: (i) the incidence angle of the IR source was varied with respect to the plane of graphene at a fixed IR power and (ii) the IR power was varied at each angle of optical incidence. Furthermore, each experiment was performed at three different electrical conditions, namely, saturation, cyclical, and sweep. In the saturation and cyclical experiments the corresponding change in the resistance (drop in the voltage) was measured by passing a constant current of 100 μA. The saturation data was acquired at a fixed IR exposure until the resistance (drop in the voltage) reached a constant value, wherein the cyclical measurements, the IR radiation was periodically exposed for a time interval of 60 s, and the corresponding changes in the resistance were recorded. In addition, the voltage was swept from −1 to 1 V before IR exposure and during electrical saturation. All the measurements were carried out at room temperature. The change in the photo induced electrical conductivity of H-graphene was estimated from the differential conductivity (dI/dV) plotted with respect to the applied bias with and without IR exposure.

2. RESULTS AND DISCUSSION

Figure 2a shows a schematic diagram of the experimental setup for the photodetection study. The H-graphene is placed between the gold electrodes, and the incident radiation is shown at various angles between 30 and 120°. Figure 2b elucidates the band diagram of H-graphene; the bandgap opening in the graphene is due to the hydrogen treatment of

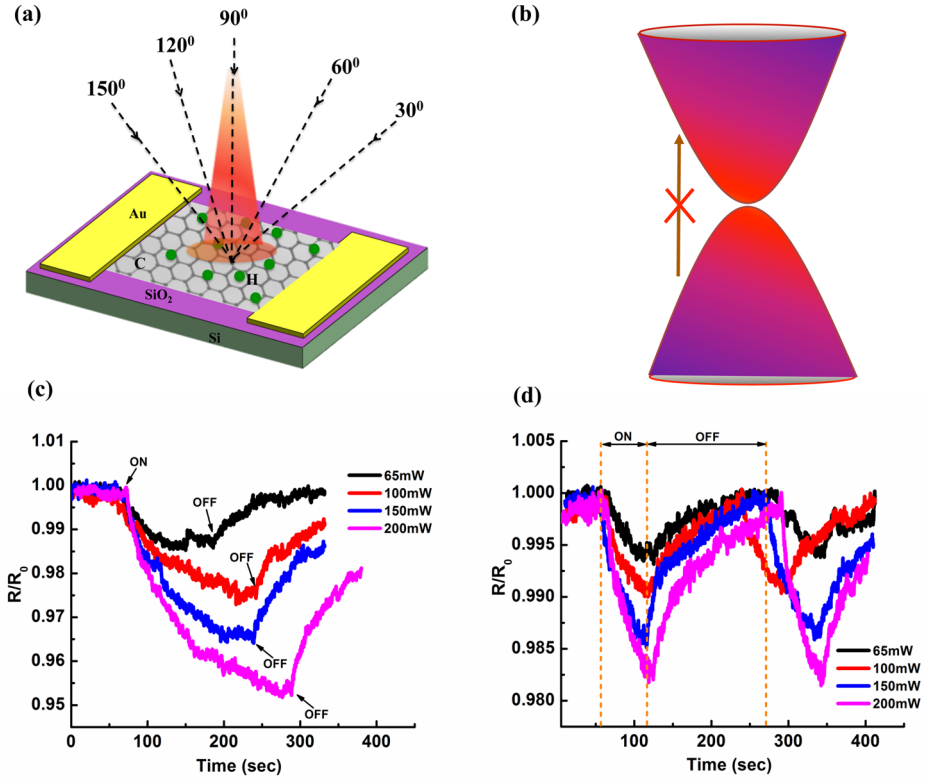

Figure 2. (a) Schematic of the experimental setup; the source meter is connected to H-graphene placed between gold electrodes, and a variation in the IR incidence angle (30−150°) is shown by arrows. (b) Schematic of the band-diagram of graphene after hydrogenation showing a band gap opening. (c) Normalized change in the resistance for saturation response. (d) Cyclic response at different IR powers at a constant incident angle of 30°.

the graphene results in reducing the carrier recombination and in turn enhances the photoresponse in H-graphene. Figure 2c illustrates the saturation response of H-graphene device as a function of exposure time for different IR powers. The normalized resistance (R/R_0) was calculated by normalizing the measured resistance (R) upon exposure with the initial resistance (R_0) measured without exposure of IR radiation. The measurement was performed at a continuous IR exposure until the photoresponse achieves a steady state and subsequently the IR radiation was turned off. Similar measurement was repeated for different IR radiation powers at a fixed incidence angle of 30°. At all incident powers, the resistance of the H-graphene device decreases exponentially as the IR was turned on. After a longer period of exposure, it tends to saturate, and the resistance recovers to its original value after the radiation was turned off. This change in resistance revealed a photoresponsivity of H-graphene device toward IR radiation. It is remarkable to note that the magnitude of photoresponse in H-graphene is 3−4 orders of magnitude higher than the earlier reported response in pristine graphene.[27] The measured change in resistance while saturation is 423, 786, 1101, and 1524 Ω for the power of 65, 100, 150, and 200 mW, respectively, while pristine graphene demonstrated a change of 133, 246, 370, and 437 Ω for the same powers, respectively.

Photoelectric current generated by excitons across the device channel mainly contributes to the photoresponse in H-graphene upon exposure to IR radiation. These excitons are generated when incident photons excite the electrons from the valence band to the conduction band; the electrons are later separated into free carriers and simultaneously accelerated by the external bias applied across the device channel in the form of photoelectric current. The enhanced photoresponse in H-graphene can be explained by considering a finite bandgap in the graphene band structure because hydrogen incorporation breaks the symmetry between the two carbon atoms in the graphene unit cell hence opens a finite gap at the Dirac point of the band structure.[28]

Thus, the enhanced photoinduced carrier lifetime of generated charge carriers increases the internal quantum efficiency of the device that resulted in improving the photoresponsivity of the device. Therefore, the performance of the H-graphene is similar to a conventional semiconductor. It is worth noting that the device takes a longer time to reach the saturation state as the radiation power increases. This could be contributed to the carrier scattering effect with the increase in IR power, the number of incident photons increases, and thus increases the rate of collision among a large number of available free carriers also enhances. Due to the multiple scattering, the carrier acceleration is limited by a change in their momentum and thus the hot carriers (both electron and holes) take a longer time to reach the electrodes.

The cyclic response of the device with the periodic exposure is elucidated in Figure 2d that reveals a high photoelastic response of the device at all incident IR powers. The exponential decay and rise of the resistances, R_1 and R_2, respectively, are fitted with the following equations:

$$R_1 = A_1 \exp\left(-\frac{t_1}{\tau_1}\right) \quad (1)$$

dx.doi.org/10.1021/am503892m | ACS Appl. Mater. Interfaces 2014, 6, 16763−16768

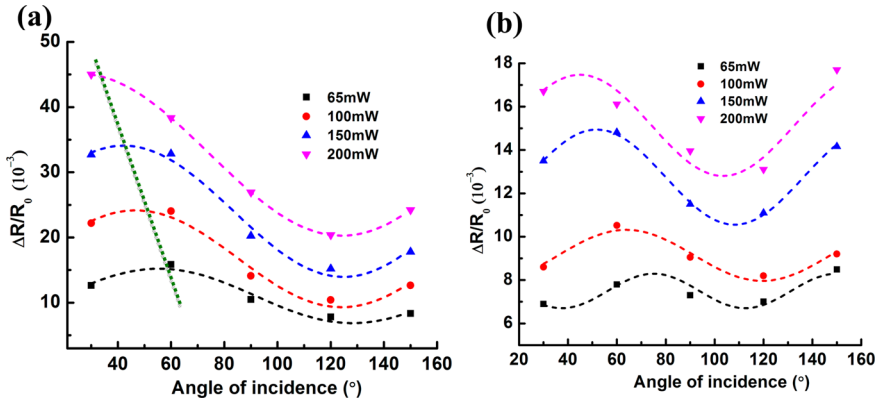

Figure 3. Normalized change in the resistance is plotted with different angle of incidences for different IR powers during (a) saturation and (b) cyclical experiments.

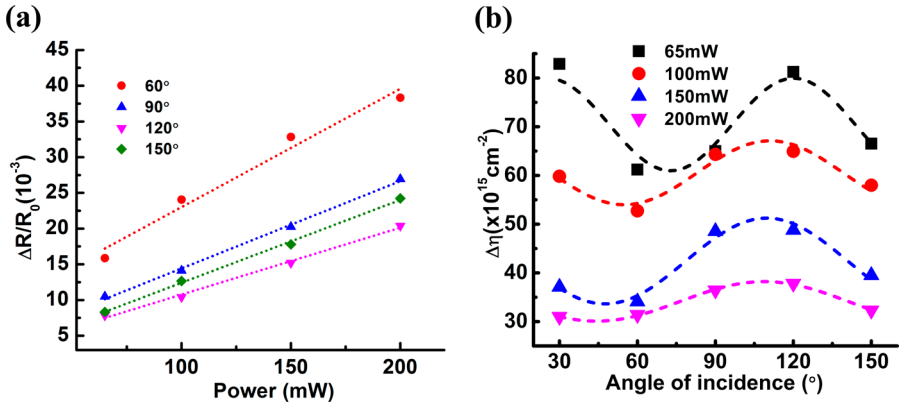

Figure 4. (a) Normalized change in the resistance as a function of IR power at different angles of IR incidence for saturation measurement and (b) change in the carrier concentration during cyclical experiments with the variation in the angle of IR incidence at different radiation power.

$$R_2 = A_2 \exp\left(-\frac{t_2}{\tau_2}\right) \quad (2)$$

where A_1 and A_2 are constants, τ_1 and τ_2 are the decay and rise time constants, respectively, for the cyclical response curve. The values of τ_1 and τ_2 are measured and found to be within a range between 35 ± 3 s and 30 ± 2 s at different powers.

The effect of optical incidence (variation in the angle of IR exposure) on the photoresponse of H-graphene device was measured with respect to the graphene plane for both the saturation and cyclic cases, as illustrated in Figure 3. In each case, the measurements were recorded for different IR powers. The normalized change in resistance, $\Delta R/R_0$ (photoresponse), where ΔR is the difference between initial resistance and the measured resistance ($R_0 - R$), varies with the sinusoidal function of the incident angle. The lowest photoresponse occurred at 120°, while the maximum response is measured at around an angle of 60°. The resulting curve for the change in electrical response ($\Delta R/R_0$) with the angle of incidence (θ) is fitted with a relationship given by $(\Delta R/R_0) = A \sin(n(\theta + \Phi))$, where A denotes the amplitude of the sinusoidal function, n is an integer, and Φ represents the phase shift dependent on the incident power. The nonlinear photoresponse of the H-graphene device with the incident angle can be understood by photon drag effect; the momentum of the absorbed photons is transferred to the free carriers through electron−phonon interaction.[29] This phenomenon is observed when the momentum relaxation rate is small due to a strong electron−phonon coupling leading to higher momentum transfer rate. The photon-drag current is highly angle-dependent because of the directed motion of the free carriers caused by the absorbed photon momentum, which is very similar to the optical rectification effect of the second order optical quadruple nonlinearity.[29] A similar effect has been observed earlier in carbon nanotube,[29] nanographite,[30] and pristine graphene.[27] Similar to that in semiconducting materials,[31−34] charge carrier generation in H-graphene takes place through interband transition when a photon is absorbed.[29] In this process, H-graphene has clearly shown a relatively higher momentum relaxation time as compared to the pristine graphene which causes an enhancement in the response of the device.

It is interesting to note that with the increase in the source power, the maximum photoresponse shifts toward the lower incident angle, as depicted in Figure 3a by a dotted line. Higher power (200 mW) showed a maximum response at 30°, and at the lower power (65 mW), the maximum photoresponse was noticed at 60°. Variation of both the power and angle of incidence of radiation is a combined method for varying the photon flux on to the graphene surface. The coupling efficiency between the angle of incidence and IR power decides the resultant photon flux, which is maximum at lower angle and higher power, and thus, a progressive shift in maximum responsivity occurred at lower angle with the increase of IR power. In the case of cyclic measurement (Figure 3b), a complete sinusoidal response was observed, but it is different from saturation measurements. The observed discrepancies are

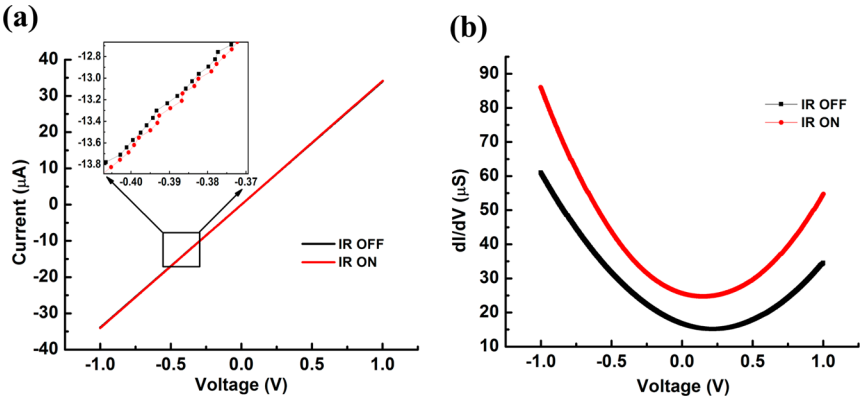

Figure 5. (a) Current−voltage (I−V) curve of H-graphene device measured before and during IR exposure, (inset) magnified I−V curve. (b) Differential conductivity derived from I−V curve for both before and during IR exposure.

due to the change in exposure time, which indicates that the exposure time is also a crucial parameter in photoresponse of H-graphene.

The optical power-dependent response of the device is extrapolated from Figure 2c and is plotted in Figure 4a. A linear increase in the photoresponse with the incident power is depicted for the saturation experiments, and a similar linear dependence response is also observed for cyclic experiments for all the angles of incidence. It is clear that higher incident power contributes greater number of incident photons and thus greater generation of excitons, which results in a higher photoelectric current and thus higher photoresponsivity. The photo generated carrier concentration is calculated by using the equation in ref 35. Figure 4b shows the change in carrier concentration as a function of angle of incidence at different IR powers during cyclical experiments. The generated curve is fitted with a cosine function given by $\Delta\eta = A\cos(n(\theta+\Phi))$, where A denotes the amplitude, n is a constant, and Φ represents the phase shift depends on the incident power, which confirms our earlier observation on the nonlinear change of resistance as was illustrated in Figure 3.

Figure 5a shows a typical current−voltage (I−V) characteristic of H-graphene device measured by sweeping voltage from −1 to +1 V, with and without IR exposure. The inset reveals a closer view of both the currents at negative bias. Overall, linear I−V characteristics are demonstrated, however, the nonlinear characteristics of I−V curves are clearly visible at lower voltage when the differential conductance (dI/dV) is plotted with respect to the voltage, as shown in Figure 5b.

As previously mentioned, the hydrogen attachment to graphene produces a mixed phase structure with a fraction of C−C sp^2 and C−H sp^3 bonding, which builds up an inhomogeneous potential distribution across the device channel while applying an external bias. The tunneling current between the two mixed phase structures results into a nonlinear I−V characteristic (Figure 5a). It is worth noting that the minima of the differential conductivity curve shift toward the charge neutrality point when the IR was turned on. This elucidates that the photogenerated carriers also produce additional electric field opposing the already existing internal field. Lee et al.[36] demonstrated an internal electric field produced by the Schottky contact between graphene−gold separates the photo-excited carriers (excitons) without applying any external bias. However, in our measurement, an external bias is required to separate the excitons, as the carrier mobility of our CVD graphene is very low (1200 $cm^2\ V^{-1}\ s^{-1}$), and thus the aforementioned self-produced internal field in the device is insufficient to separate the electron−hole pairs before they recombine.

3. CONCLUSION

An enhanced photoresponse in a H-graphene photodetector is demonstrated. The photoresponse of H-graphene is measured nearly 3−4 times higher than that of pristine graphene. A linear photoresponse with IR powers is observed for both saturation and cyclic measurements, whereas a nonlinear response is recorded with the change in optical angle of the incident radiation. The enhanced photoresponse of H-graphene is understood from the phenomenon of bandgap opening in graphene due to the hydrogen attachment in the graphene lattice. Our results clearly indicate that the IR response of H-graphene is mainly due to the photon drag effect. The photoresponse of H-graphene detector could be further enhanced by engineering the bandgap more precisely and adding the different functionality to the graphene.

4. EXPERIMENTAL METHODS

4.1. Graphene Growth and Transfer. Large-area, single-layer graphene was grown by CVD on a 25 μm thick copper foil of 99.89% purity (Alfa Aesar). Before carrying out the growth process, we evacuated the chamber to a low pressure of 10^{-2} Torr, flushed it with argon gas for 25 min at a flow rate of 400 sccm (standard cubic centimeters per minute), and then purged hydrogen gas (100 sccm) for 10 min. The copper substrate was annealed for 30 min in the presence of hydrogen gas at a temperature of 980 °C. Subsequently, graphene growth was carried out in the presence of methane (18 sccm) and hydrogen gases (54 sccm) was flown for 30 min at a pressure of 20 Torr. Finally, the methane flow was stopped, and the chamber was allowed to cool in the presence of hydrogen gas. Polymer methyl methacrylate (PMMA)-assisted wet transfer technique was employed to transfer graphene from the copper substrate on to a 300 nm thick silicon dioxide coated p-type silicon substrate.

4.2. Hydrogenation of Graphene. The hydrogenation of the graphene was performed in a high-vacuum (2×10^{-9} Torr) reactive ion etching system. Hydrogen plasma was generated between the cathode and an anode by controlling the source power (100 W) and gas pressure (15 mTorr). The hydrogen plasma exposure time was optimized and maintained for 2s.

4.3. Device Fabrication and Electrical Measurements. The H-graphene photodetector was fabricated by depositing Cr (5 nm)/Au (50 nm) electrodes on the H-graphene samples with a separation of ~2.5 mm. A constant bias current (Keithley 2011A) of 100 μA was applied across the device, and the resulting potential drop (resistance change) was measured using a data acquisition system. The

photodetection experiment was conducted using an IR source with an optical fiber (core diameter ~8 μm and wavelength ~1550 nm). The photodetector measurements were carried out by varying IR powers and incident angles.

AUTHOR INFORMATION

Corresponding Author

*E-mail: abha.misra1@gmail.com. Tel: +91-8022933198.

Author Contributions

The manuscript was written through contributions of all authors. All authors have given approval to the final version of the manuscript.

Notes

The authors declare no competing financial interest.

REFERENCES

(1) Urich, A.; Unterrainer, K.; Mueller, T. Intrinsic Response Time of Graphene Photodetectors. *Nano Lett.* **2011**, *11*, 2804−2808.

(2) Xia, F.; Mueller, T.; Lin, Y.-M.; Valdes-Garcia, A.; Avouris, P. Ultrafast Graphene Photodetector. *Nat. Nanotechnol.* **2009**, *4*, 839−843.

(3) Mueller, T.; Xia, F.; Avouris, P. Graphene Photodetectors for High-speed Optical Communications. *Nat. Photonics* **2010**, *4*, 297−301.

(4) Sun, D.; Aivazian, G.; Jones, A. M.; Yao, W.; Cobden, D.; Xu, X. New Aspects of Photocurrent Generation at Graphene pn Junctions Revealed by Ultrafast Optical Measurements. *Bull. Am. Phys. Soc.* **2012**, *57*, arXiv:1108.3360.

(5) Gan, X.; Shiue, R.-J.; Gao, Y.; Meric, I.; Heinz, T. F.; Shepard, K.; Hone, J.; Assefa, S.; Englund, D. Chip-Integrated Ultrafast Graphene Photodetector with High Responsivity. *Nat. Photonics* **2013**, *7*, 883−887.

(6) Liu, C.−H.; Chang, Y.−C.; Norris, T. B.; Zhong, Z. Graphene Photodetectors with Ultra-Broadband and High Responsivity at Room Temperature. *Nat. Nanotechnol.* **2014**, *9*, 273−278.

(7) Gowda, P.; Sakorikar, T.; Reddy, S. K.; Ferry, D. B.; Misra, A. Defect-Induced Enhancement and Quenching Control of Photocurrent in Few-Layer Graphene Photodetectors. *ACS Appl. Mater. Interfaces* **2014**, *6*, 7485−7490.

(8) Mueller, T.; Xia, F.; Freitag, M.; Tsang, J.; Avouris, P. Role of Contacts in Graphene Transistors: A Scanning Photocurrent Study. *Phys. Rev. B: Condens. Matter Mater. Phys.* **2009**, *79*, 245430−245436.

(9) Xia, F.; Mueller, T.; Mojarad, R. G.; Freitag, M.; Lin, Y.-M.; Tsang, J.; Perebeinos, V.; Avouris, P. Photocurrent Imaging and Efficient Photon Detection in a Graphene Transistor. *Nano Lett.* **2009**, *9*, 1039−1044.

(10) Kim, C. O.; Kim, S.; Shin, D. H.; Kang, S. S.; Kim, J. M.; Jang, C. W.; Joo, S. S.; Lee, J. S.; Kim, J. H.; Choi, S.-H.; et al. High Photoresponsivity in an All-Graphene p−n Vertical Junction Photodetector. *Nat. Commun.* **2014**, *5*, 3249.

(11) Lemme, M. C.; Koppens, F. H. L.; Falk, A. L.; Rudner, M. S.; Park, H.; Levitov, L. S.; Marcus, C. M. Gate-Activated Photoresponse in a Graphene p-n Junction. *Nano Lett.* **2011**, *11*, 4134−4137.

(12) Lu, X.; Vaillancourt, J.; Meisner, M. J. A Modulation-Doped Longwave Infrared Quantum Dot Photodetector with High Photoresponsivity. *Semicond. Sci. Technol.* **2007**, *22*, 993−996.

(13) Li, J.; Niu, L.; Zheng, Z.; Yan, F. Photosensitive Graphene Transistors. *Adv. Mater.* **2014**, *26*, 5239−5273.

(14) Echtermeyer, T. J.; Britnell, L.; Jasnos, P. K.; Lombardo, A.; Gorbachev, R. V.; Grigorenko, A. N.; Geim, A. K.; Ferrari, A. C.; Novoselov, K. S. Strong Plasmonic Enhancement of Photovoltage in Graphene. *Nat. Commun.* **2011**, *2*, 458.

(15) Kim, K.; Choi, J.-Y.; Kim, T.; Cho, S.-H.; Chung, H.-J. A Role for Graphene in Silicon-Based Semiconductor Devices. *Nature* **2011**, *479*, 338−344.

(16) Craciun, M. F.; Khrapach, I.; Barnes, M. D.; Russo, S. Properties and Applications of Chemically Functionalized Graphene. *J. Phys.: Condens. Matter* **2013**, *25*, 423201−423223.

(17) Withers, F.; Russo, S.; Dubois, M.; Craciun, M. F. Tuning the Electronic Transport Properties of Graphene through Functionalisation with Fluorine. *Nanoscale Res. Lett.* **2011**, *6*, 526−537.

(18) Guo, B.; Fang, L.; Zhang, B.; Gong, J. R. Graphene Doping: A Review. *Insciences J.* **2011**, *1*, 80−89.

(19) Craciuna, M. F.; Russo, S.; Yamamotoc, M.; Tarucha, S. Tunable Electronic Properties in Graphene. *Nano Today* **2011**, *6*, 42−60.

(20) Flores, M. Z. S.; Autreto, P. A. S.; Legoas, S. B.; Galvao, D. S. Graphene to Graphane: A Theoretical Study. *Nanotechnology* **2009**, *20*, 465704−465710.

(21) Casolo, S.; Lovvik, O. M.; Martinazzo, R.; Tantardini, G. F. Understanding Adsorption of Hydrogen Atoms on Graphene. *J. Chem. Phys.* **2009**, *130*, 054704−054714.

(22) Elias, D. C.; Nair, R. R.; Mohiuddin, T. M. G.; Morozov, S. V.; Blake, P.; Halsall, M. P.; Ferrari, A. C.; Boukhvalov, D. W.; Katsnelson, M. I.; Geim, A. K.; et al. Control of Graphene's Properties by Reversible Hydrogenation. *Science* **2009**, *323*, 610−613.

(23) Ferrari, A. C.; Basko, D. M. Raman Spectroscopy as a Versatile Tool for Studying the Properties of Graphene. *Nat. Nanotechnol.* **2013**, *8*, 235−246.

(24) Ferreira, E. H. M.; Moutinho, M. V. O.; Stavale, F.; Lucchese, M. M.; Capaz, R. B.; Achete, C. A.; Jorio, A. Evolution of the Raman Spectra from Single-, Few-, and Many-layer Graphene with Increasing Disorder. *Phys. Rev. B: Condens. Matter Mater. Phys.* **2010**, *82*, 125429−125438.

(25) Lucchese, M. M.; Stavale, F.; Ferreira, E. H. M.; Vilania, C.; Moutinho, M. V. O.; Capaz, R. B.; Achete, C. A.; Jorio, A. Quantifying Ion-Induced Defects and Raman Relaxation Length in Graphene. *Carbon* **2010**, *48*, 1592−1597.

(26) Kim, K.-J.; Choi, J.; Lee, H.; Lee, H.-K.; Kang, T.-H.; Han, Y.-H.; Lee, B.-C.; Kim, S.; Kim, B. Effects of 1 MeV Electron Beam Irradiation on Multilayer Graphene Grown on 6H-SiC(0001). *J. Phys. Chem. C* **2008**, *112*, 13062−13064.

(27) Gowda, P.; Mohapatra, D. R.; Misra, A. Nonlinear Optical Absorption in Graphene Infrared Photodetector. *Nanotechnology* **2014**, *25*, 335710−335716.

(28) Giovannetti, G.; Khomyakov, P. A.; Brocks, G.; Kelly, P. J.; Brink, J. v. d. Substrate-Induced Bandgap in Graphene on Hexagonal Boron Nitride: Ab Initio Density Functional Calculations. *Phys. Rev. B: Condens. Matter Mater. Phys.* **2007**, *76*, 073103−073107.

(29) Obraztsov, A. N.; Lyashenko, D. A.; Fang, S.; Baughman, R. H.; Obraztsov, P. A.; Garnov, S. V.; Svirko, Y. P. Photon Drag Effect in Carbon Nanotube Yarns. *Appl. Phys. Lett.* **2009**, *94*, 2311121−2311124.

(30) Obraztsov, P. A.; Mikheev, G. M.; Garnov, S. V.; Obraztsov, A. N.; Svirko, Y. P. Polarization-Sensitive Photoresponse of Nanographite. *Appl. Phys. Lett.* **2011**, *98*, 0919031−0919034.

(31) Grinberg, A. A.; Luryi, S. Theory of the Photon−Drag Effect in a Two−Dimensional Electron Gas. *Phys. Rev. B: Condens. Matter Mater. Phys.* **1988**, *38*, 87−96.

(32) Panyakeow, S.; Shirafuji, J.; Inuishi, Y. Photon Drag Effect in p-Type Tellurium at 10.6 m. *Appl. Phys. Lett.* **1975**, *46*, 1245−1251.

(33) Valov, P. M.; Ryvkin, B. S.; Ryvkin, S. M.; Yaroshetskii, I. D. An Anisotropic Photon Drag Effect in Nonspherical-Band Cubic Semiconductors. *Phys. Status Solidi B* **1972**, *53*, 65−70.

(34) Loudon, R.; Barnett, S. M.; Baxter, C. Radiation Pressure and Momentum Transfer in Dielectrics: The Photon Drag Effect. *Phys. Rev. A: At., Mol., Opt. Phys.* **2005**, *71*, 063802−063813.

(35) Kurra, N.; Bhadram, V. S.; Narayana, C.; Kulkarni, G. U. Few Layer Graphene to Graphitic Films: Infrared Photoconductive versus Bolometric Response. *Nanoscale* **2012**, *5*, 381−389.

(36) Lee, E. J. H.; Balasubramanian, K.; Weitz, R. T.; Burghard, M.; Kern, K. Contact and Edge Effects in Graphene Devices. *Nat. Nanotechnol.* **2008**, *3*, 486−490.